Investigation of Carrier Transport Mechanism in High Mobility ZnON Thin-Film Transistors

Chan-Yong Jeong, Hee-Joong Kim, Dae-Hwan Kim, Hyun-Suk Kim, Tae Sang Kim, Jong-Baek Seon, Sunhee Lee, Dae Hwan Kim, and Hyuck-In Kwon

***Abstract*— In this letter, the carrier transport mechanism in a high-mobility zinc oxynitride (ZnON) thin-film transistor (TFT) is investigated by analyzing the gate bias and temperature dependence of conductance and intrinsic field-effect mobility (μ_{FEi}) in the subthreshold and above-threshold regions, respectively. The measured drain currents increase with a temperature and show a thermally activated Arrhenius-like behavior in the subthreshold region. The experimental results are well explained using a Meyer–Neldel rule, which suggests that the trap-limited conduction is the dominant carrier transport mechanism in the ZnON TFT in the subthreshold region. The carrier transport mechanism in the ZnON TFT in the above-threshold region is investigated by examining the gate overdrive voltage (V_{OV}) and temperature dependence of μ_{FEi}. μ_{FEi} extracted from the ZnON TFT decreases with an increase in V_{OV} and temperature, which suggests that the phonon scattering is the most probable mechanism limiting μ_{FEi} in the ZnON TFT in the above-threshold region.**

***Index Terms*— Carrier transport mechanism, zinc oxynitride thin-film transistor, Meyer-Neldel rule, trap-limited conduction, phonon scattering.**

I. Introduction

OF LATE, zinc oxynitride (ZnON) is attracting a considerable attention as a channel material of the high-mobility thin-film transistor (TFT) for next-generation large-size, high-resolution, and high-frame rate displays [1], [2]. ZnON TFTs exhibit a high field-effect mobility (μ_{FE}) of ~100 cm^2/V·s owing to the small effective mass of an electron in ZnON [2], [3]. In addition, the substitution of oxygen with nitrogen in ZnO reduces the energy band gap to 1.3 eV, which eliminates the deep levels near the valence band maximum formed by oxygen vacancies. Therefore, a significant improvement in photo-stability has been reported in ZnON TFTs compared to the multi-cation amorphous oxide TFTs including amorphous indium-gallium-zinc oxide (a-IGZO) TFTs [4]. In the last several years, various studies have been performed to improve the electrical performances of ZnON TFTs [1]–[11]. However, the carrier transport mechanism in the ZnON TFT remains under debate even though the impurity scattering [1], percolation conduction [2], and trap-limited conduction [9] have been considered as possible carrier transport mechanisms in the ZnON TFTs. Knowledge about the carrier transport mechanism is essential for both obtaining a fundamental understanding of the device operation and improving the device performances. In this work, we systematically investigate the carrier transport mechanism in the ZnON TFT by analyzing the gate bias and temperature dependence of conductance and intrinsic field-effect mobility (μ_{FEi}) in the subthreshold and above-threshold regions, respectively.

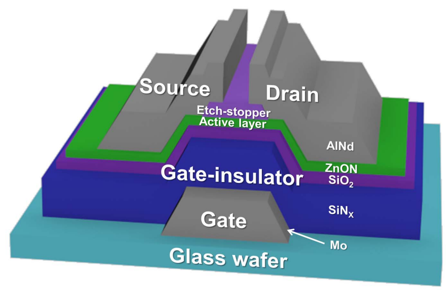

Fig. 1. Cross-sectional view of the fabricated ZnON TFT.

II. Device Fabrication

In this study, experiments were performed in the ZnON TFT with an inverted-staggered and etch-stopper structure. The fabrication procedure of the device is as follows. A Mo (200 nm) gate was patterned on a glass substrate, and then a SiN_X (350 nm)/SiO_2 (50 nm) was formed by plasma-enhanced chemical vapor deposition (PECVD). Next, a ZnON thin-film (50 nm) was grown by sputtering and then patterned. The ZnON channel area was protected by an etch-stopper layer of SiO_2 (100 nm) to prevent damage to the back channel during the etching process of source/drain electrodes. The deposition of the ZnON thin-film was performed using a Zn metal target at a gas flow rate of $Ar/N_2/O_2$ = 10/100/2. In sequence, a source/drain of AlNd was patterned by dry etching, and the TFT was passivated by the SiO_2 passivation layer. Fig. 1 depicts a cross-sectional view of the fabricated ZnON TFT. The electrical parameters of the fabricated ZnON TFT extracted from the device with a

Manuscript received August 2, 2016; revised October 12, 2016; accepted October 18, 2016. Date of publication October 20, 2016; date of current version November 22, 2016. This work was supported by the National Research Foundation of Korea (NRF) funded by the Korean Government (MSIP) under Grant 2014-005368 and 2016R1A5A1012966. The review of this letter was arranged by Editor A. Flewitt. *(Corresponding authors: Dae Hwan Kim and Hyuck-In Kwon.)*

C.-Y. Jeong, H.-J. Kim, D.-H. Kim, and H.-I. Kwon are with the School of Electrical and Electronics Engineering, Chung-Ang University, Seoul 156-756, South Korea (e-mail: hyuckin@cau.ac.kr).

H.-S. Kim is with the Department of Material Science and Engineering, Chungnam National University, Daejeon 305-764, South Korea.

T. S. Kim, J.-B. Seon, and S. Lee are with the Samsung Advanced Institute of Technology, Suwon 448-803, South Korea.

D. H. Kim is with the School of Electrical Engineering, Kookmin University, Seoul 136-702, South Korea (e-mail: drlife@kookmin.ac.kr).

Color versions of one or more of the figures in this letter are available online at http://ieeexplore.ieee.org.

Digital Object Identifier 10.1109/LED.2016.2619684

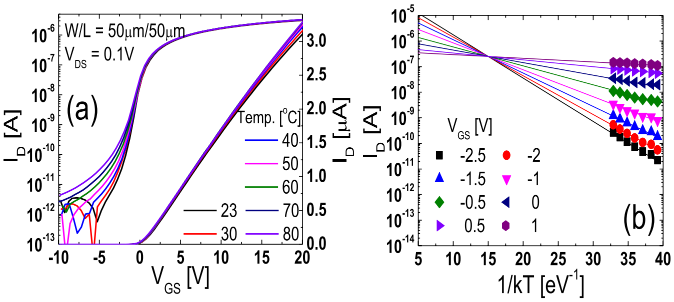

Fig. 2. (a) Transfer curves of the ZnON TFT measured by increasing the temperature from RT (23 °C) to 80 °C. (b) I_D versus $1/kT$ plot depicted as a function of V_{GS} in the subthreshold region.

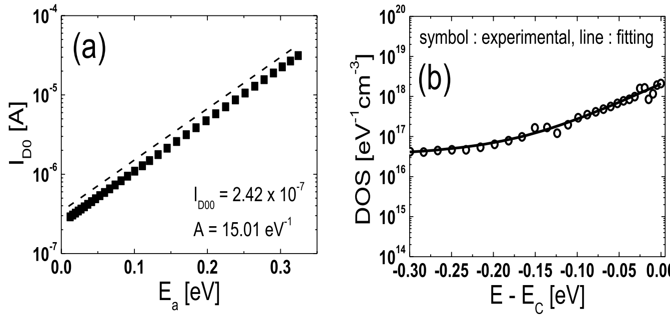

Fig. 3. (a) Variation of I_{D0} depicted as a function of E_a, where I_{D0} is the prefactor and E_a is the activation energy. (b) Surface energy distribution of the subgap DOS extracted from the temperature-dependent field-effect characteristics of the fabricated ZnON TFT based on the MN rule.

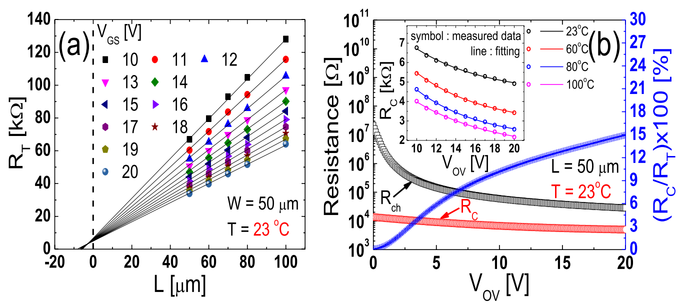

Fig. 4. (a) R_Ts plotted as a function of L for different V_{GS}s. (b) R_C, R_{ch}, and R_C/R_T plotted as a function of V_{GS}. Measurements were made for a device with a W/L of 50 μm/50 μm at RT. The inset depicts the temperature dependence of R_C extracted at various V_{OV}s.

width/length (W/L) of 50 μm/50 μm are as follows: a μ_{FE} of 119.2 cm^2/V·s, threshold voltage (V_{th}) of 0.6 V, subthreshold slope (SS) of 0.62 V/dec, and turn-on voltage (V_{on}) of −5.2 V. The μ_{FE} of the fabricated ZnON TFT is higher than μ_{FE}s of the previously reported ZnON TFTs (∼40 – 100 cm^2/V·s [8]–[12]) and conventional a-IGZO TFTs (∼10 – 20 cm^2/V·s [13]). Here, μ_{FE} was extracted from the maximum transconductance at a drain-to-source voltage (V_{DS}) of 0.1 V and V_{th} was determined by the intercept of the extrapolated curve with a voltage axis. V_{on} was defined as the onset voltage at which the drain current (I_D) increases.

III. Results and Discussion

Fig. 2(a) presents the transfer curves of the ZnON TFT measured by increasing the temperature from RT (23 °C) to 80 °C. Measurements were performed in air, and the device was placed on the heated chuck which was set at the measurement temperature for 30 mins for thermal equilibrium. Fig. 2(a) shows that V_{on} moves in the negative direction and SS continuously increases with an increase of temperature. I_D in the above-threshold region exhibits an almost constant value in all measurement temperatures. The temperature-dependent variation in the transfer curve was reversible because it recovered to the initial one when the temperature decreased to RT. Fig. 2(b) presents the I_D versus $1/kT$ plot depicted as a function of the gate-to-source voltage (V_{GS})in the subthreshold region, where T is the temperature and k is the Boltzmann constant. Fig. 2(b) shows that the temperature dependence of I_D can be expressed by the Arrhenius equation of

$$I_D = I_{D0}\exp(-E_a/kT), \quad (1)$$

where I_{D0} is the prefactor and E_a is the activation energy. I_{D0} and E_a can be extracted from Fig. 2(b) as a function of V_{GS}. Fig. 3(a) shows the variation of I_{D0}plotted as a function of E_a, which denotes that I_{D0} increases exponentially with E_a. It obeysthe Meyer-Neldel (MN) rule, which is the intrinsic property of a disordered semiconductor [14]–[17]. Similar experimental results were reported in a-IGZO TFTs in the subthreshold region [18], [19]. The MN rule has been explained by a trap-limited conduction model and a statistical shift of the Fermi level [16]–[19]. The experimental data in Fig. 3(a) show that the dominant carrier transport mechanism in the ZnON TFT in the subthreshold region is the trap-limited conduction. Eq. (2) is the MN equation

$$I_{D0} = I_{D00}\exp(A \cdot E_a), \quad (2)$$

where I_{D00} is the prefactor for I_{D0} and$A$ is the characteristic MN parameter. From Eq. (2) and the experimental data in Fig. 3(a), an almost constant value of A (15.01 eV^{-1}) is obtained over E_as between 0.02 and 0.32 eV. In the trap-limited conduction model, the conduction characteristics are strongly affected by multiple trapping and thermal release events associated with the localized tail states. As the temperature increases, more carriers are thermally activated from the trap sites to the conduction band, and they move quickly to the drain electrode on account of the lateral electric field. Fig. 3(b) shows the surface energy distribution of the subgap density of states (DOS) extracted from the temperature-dependent field-effect characteristics of the fabricated ZnON TFT in the subthreshold region based on the MN rule [18], [19].

To investigate the intrinsic carrier transport mechanism in the ZnON TFT in the above-threshold region, μ_{FEi} of the device was extracted using the transmission line method [20]. In Fig. 4(a), the total resistances between the source and drain electrodes of the TFT (R_Ts) are plotted as a function of L for different V_{GS}s. The contact resistance (R_C) is extracted from the R_T-axis intercept as a function of V_{GS}, and μ_{FEi} is obtained by Eq. (3) after excluding the contact resistance effects.

$$\mu_{FEi} = \frac{\partial I_D}{\partial V_{GS}} \cdot \frac{1}{(W/L)C_i(V_{DS} - I_D R_C)}, \quad (3)$$

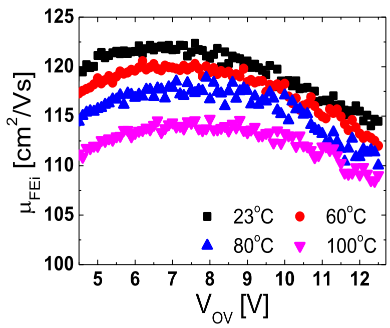

Fig. 5. V_{OV} and temperature dependence of μ_{FEi} extracted from the ZnON TFT in the above-threshold voltage region.

where, C_i is the gate dielectric capacitance per unit area. Fig. 4(b) compares R_C and the channel resistance (R_{ch}) extracted from the device with a W/L of 50 μm/50 μm at RT, and calculates R_C/R_T as a function of V_{GS}, where $R_T = R_{ch} + R_C$. The width-normalized contact resistances calculated from the extracted R_Cs in Fig. 4(b) are similar with those of a-IGZO TFTs [21]–[23]. Fig. 4(b) shows that the contribution of R_C continuously increases with an increase of the gate overdrive voltage ($V_{OV} = V_{GS} - V_{th}$). It shows that R_C must be considered when extracting μ_{FEi} in the fabricated ZnON TFT. The inset of Fig. 4(b) depicts the temperature dependence of R_C extracted at various V_{OV}s. R_C decreases with an increase of temperature because the carriers more easily overcome the Schottky barrier between the AlNd and ZnON at a higher temperature.

Fig. 5 depicts the V_{OV} and temperature dependence of μ_{FEi} extracted by Eq. (3) from the fabricated ZnON TFT. In multi-cation amorphous oxide TFTs, including a-IGZO TFTs, the carrier transport has been mainly explained based on the trap-limited and percolation conduction mechanisms [24]–[26]. Fig. 5 shows that μ_{FEi} decreases with an increase in V_{OV} and temperature. Because μ_{FEi} increases with V_{OV} and temperature when it is determined by trap-limited or percolation conduction mechanisms [27], the experimental results in Fig. 5 show that the carrier transport in the ZnON TFT in the above-threshold region is predominantly not governed by these mechanisms. The unavailability of the percolation conduction mechanism in explaining the carrier transport in the ZnON TFT is physically acceptable because the ZnON is free from the potential fluctuation in the conduction band minima resulting from the interactions of multiple cations [5]. The decrease of μ_{FEi} with an increase in V_{OV} and temperature is observed when μ_{FEi} is limited by the phonon scattering [28]. The decrease of μ_{FEi} with an increase in V_{OV} is also observed when the carrier transport is limited by the surface roughness scattering. However, the effects of temperature on the surface roughness scattering are known to be negligible [28]. The phonon scattering is the representative scattering mechanism governing the band transport of carriers, and has been considered as the dominant mechanism limiting the mobility in the single crystalline metal-oxide-semiconductor field-effect transistor [29] and the multilayer molybdenum disulfide transistor [30]. Based on the experimental results in Fig. 5, the phonon scattering is believed to be the most probable mechanism limiting μ_{FEi} in the fabricated high-mobility ZnON TFT in the above-threshold region.

IV. Conclusion

In this letter, the gate bias and temperature dependence of the conductance and μ_{FEi} were analyzed to investigate the carrier transport mechanism in the ZnON TFT. In the subthreshold region, V_{on} moves in the negative direction and *SS* continuously increases with an increase of temperature. The measured bias-temperature dependence of the conductance is well explained by the MN rule, which suggests that the dominant carrier transport mechanism in the ZnON TFT in the subthreshold region is the trap-limited conduction caused by the multiple trapping and thermal release events associated with the localized tail states. The carrier transport mechanism in the ZnON TFT in the above-threshold region was investigated by observing the bias-temperature dependence of μ_{FEi}. μ_{FEi}s were extracted by excluding the contact resistance effects using the transmission line method. According to the results, μ_{FEi} decreases with an increase in V_{OV} and temperature, which suggests that the carrier transport is mainly limited by the phonon scattering in the ZnON TFT in the above-threshold region.

References

[1] Y. Ye, R. Lim, and J. M. White, "High mobility amorphous zinc oxynitride semiconductor material for thin film transistors," *J. Appl. Phys.*, vol. 106, no. 7, p. 074512, 2009, doi: 10.1063/1.3236663.

[2] H.-S. Kim, S. H. Jeon, J. S. Park, T. S. Kim, K. S. Son, J.-B. Seon, S.-J. Seo, S.-J. Kim, E. Lee, J. G. Chung, H. Lee, S. Han, M. Ryu, S. Y. Lee, and K. Kim, "Anion control as a strategy to achieve high-mobility and high-stability oxide thin-film transistors," *Sci. Rep.*, vol. 3, pp. 1459-1–1459-7, Mar. 2013, doi: 145910.1038/srep01459.

[3] E. Lee, T. Kim, A. Benayad, H. Kim, S. Jeon, and G.-S. Park, "Ar plasma treated ZnON transistor for future thin film electronics," *Appl. Phys. Lett.*, vol. 107, no. 12, pp. 122105-1–122105-5, Sep. 2015, doi: 10.1063/1.4930827.

[4] J.-T. Jang, J. Park, B.-D. Ahn, D.-M. Kim, S.-J. Choi, H.-S. Kim, and D. H. Kim, "Study on the photoresponse of amorphous In–Ga–Zn–O and zinc oxynitride semiconductor devices by the extraction of sub-gap-state distribution and device simulation," *ACS Appl. Mater. Interfaces*, vol. 7, no. 28, pp. 15570–15577, Jun. 2015, doi: 10.1021/acsami.5b04152.

[5] Y. Ye, R. Lim, H. You, E. Scheer, A. Gaur, H.-C. Hsu, J. Liu, D. K. Yim, A. Hosokawa, and J. M. White, "Development of high mobility zinc oxynitride thin film transistors," *SID Symp. Dig. Tech. Papers*, vol. 44, no. 1, pp. 14–17, Jun. 2013, doi: 10.1002/j.2168-0159.2013.tb06127.x.

[6] M. Wang, L. Zhang, D. Wang, L. Yan, G. Yuan, and G. Wang, "High mobility zinc oxynitride TFT for AMOLED," *SID Symp. Dig. Tech. Papers*, vol. 45, no. 1, pp. 949–951, Jun. 2014, doi: 10.1002/j.2168-0159.2014.tb00246.x.

[7] T. S. Kim, H.-S. Kim, J. S. Park, K. S. Son, E. S. Kim, J.-B. Seon, S. Lee, S.-J. Seo, S.-J. Kim, S. Jun, K. M. Lee, D. J. Shin, J. Lee, C. Jo, S.-J. Choi, D. M. Kim, D. H. Kim, M. Ryu, S.-H. Cho, and Y. Park, "High performance gallium-zinc oxynitride thin film transistors for next-generation display applications," in *IEDM Dig. Tech. papers*, Dec. 2013, pp. 660–662, doi: 10.1109/IEDM.2013.6724701.

[8] K.-C. Ok, H.-J. Jeong, H.-S. Kim, and J.-S. Park, "Highly stable ZnON thin-film transistors with high field-effect mobility exceeding 50 cm^2/Vs," *IEEE Electron Device Lett.*, vol. 36, no. 1, pp. 38–40, Jan. 2015, doi: 10.1109/LED.2014.2365614.

[9] S. Lee, A. Nathan, Y. Ye, Y. Guo, and J. Robertson, "Localized tail states and electron mobility in amorphous ZnON thin film transistors," *Sci. Rep.*, vol. 5, pp. 13467-1–13467-9, Aug. 2015, doi: 10.1038/srep13467.

[10] K.-C. Ok, H.-J. Jeong, H.-M. Lee, J. Park, and J.-S. Park, "Comparative studies on the physical and electronic properties of reactively sputtered ZnO and ZnON semiconductors," *Ceramics Int.*, vol. 41, no. 10, pp. 13281–13284, Dec. 2015, doi: 10.1016/j.ceramint.2015.07.110.

[11] C. I. Kuan, H. C. Lin, P. W. Li, and T. Y. Huang, "High-performance submicrometer ZnON thin-film transistors with record field-effect mobility," *IEEE Electron Device Lett.*, vol. 37, no. 3, pp. 303–305, Mar. 2016, doi: 10.1109/LED.2016.2518404.

[12] E. Lee, T. Kim, A. Benayad, J. Hur, G.-S. Park, and S. Jeon, "High mobility and high stability glassy metal-oxynitride materials and devices," *Sci. Rep.*, vol. 6, pp. 23940-1–23940-10, Apr. 2016, doi: 10.1038/srep23940.

[13] S. Oh, J. H. Baeck, H. S. Shin, J. U. Bae, K. S. Park, and I. B. Kang, "Comparison of top-gate and bottom-gate amorphous InGaZnO thin-film transistors with the same SiO_2/a-InGaZnO/SiO_2 stack," *IEEE Electron Device Lett.*, vol. 35, no. 10, pp. 1037–1039, Oct. 2014, doi: 10.1109/LED.2014.2351492.

[14] W. Meyer and H. Neldel, "Relation between the energy constant and the quantity constant in the conductivity-temperature formula of oxide semiconductors," *Z. Tech. Phys.*, vol. 18, no. 12, pp. 588–593, 1937.

[15] H. Overhof and P. Thomas, *Electronic Transport in Hydrogenated Amorphous Semiconductors*. Berlin, Germany: Springer, 1989.

[16] W. B. Jackson, "Connection between the Meyer-Neldel relation and multiple-trapping transport," *Phys. Rev. B*, vol. 38, no. 5, pp. 3595–3598, Aug. 1988, doi: 10.1103/PhysRevB.38.3595.

[17] D. Guo, T. Miyadera, S. Ikeda, T. Shimada, and K. Saiki, "Analysis of charge transport in a polycrystalline pentacene thin film transistor by temperature and gate bias dependent mobility and conductance," *J. Appl. Phys.*, vol. 102, no. 2, pp. 023706-1–023706-8, Jul. 2007, doi: 10.1063/1.2753671.

[18] C. Chen, K. Abe, H. Kumomi, and J. Kanicki, "Density of states of a-InGaZnO from temperature-dependent field-effect studies," *IEEE Trans. Electron Devices*, vol. 56, no. 6, pp. 1177–1183, Jun. 2009.

[19] J. Jeong, J. K. Jeong, J.-S. Park, Y.-G. Mo, and Y. Hong, "Meyer- Neldel rule and extraction of density of states in amorphous indium-gallium-zinc-oxide thin-film transistor by considering surface band bending," *Jpn. J. Appl. Phys.*, vol. 49, no. 3s, pp. 03CB02-1–03CB02-6, Mar. 2010, doi: 10.1143/JJAP.49.03CB02.

[20] J. Kanicki, F. R. Libsch, J. Griffith, and R. Polastre, "Performance of thin hydrogenated amorphous silicon thin-film transistors," *Appl. Phys. Lett.*, vol. 69, no. 4, pp. 2339–2345, 1991, doi: 10.1063/1.348716.

[21] R. I. Kondratyuk, K. Im, D. Stryakhilev, C. G. Choi, M.-G. Kim, H. Yang, H. Park, Y. G. Mo, H. D. Kim, and S. S. Kim, "A study of parasitic series resistance components in In-Ga-Zn-oxide (a-IGZO) thin-film transistors," *IEEE Electron Device Lett.*, vol. 32, no. 4, pp. 503–505, Apr. 2011, doi: 10.1109/LED.2011.2104937.

[22] H. Bae, S. Kim, M. Bae, J. S. Shin, D. Kong, H. Jung, J. Jang, J. Lee, D. H. Kim, and D. M. Kim, "Extraction of separated source and drain resistances in amorphous indium-gallium-zinc oxide TFTs through $C - V$ characterization," *IEEE Electron Device Lett.*, vol. 32, no. 6, pp. 761–763, Jun. 2011, doi: 10.1109/LED.2011.2127438.

[23] A. Valletta, G. Fortunato, L. Mariucci, P. Barquinha, R. Martins, and E. Fortunato, "Contact effects in amorphous InGaZnO thin film transistors," *J. Display Technol.*, vol. 10, no. 11, pp. 956–961, Nov. 2014, doi: 10.1109/JDT.2014.2328376.

[24] K. Nomura, H. Ohta, A. Takagi, T. Kamiya, M. Hirano, and H. Hosono, "Room-temperature fabrication of transparent flexible thin-film transistors using amorphous oxide semiconductors," *Nature*, vol. 432, no. 4016, pp. 488–492, Nov. 2004. doi: 10.1038/nature03090.

[25] M. Bae, K. M. Lee, E.-S. Cho, H.-I. Kwon, D. M. Kim, and D. H. Kim, "Analytical current and capacitance models for amorphous indium-gallium-zinc-oxide thin-film transistors," *IEEE Trans. Electron Devices*, vol. 60, no. 10, pp. 3465–3473, Oct. 2013. doi: 10.1109/TED.2013.2278033.

[26] S. Lee, K. Ghaffarzadeh, A. Nathan, J. Robertson, S. Jeon, C. Kim, I.-H. Song, and U.-I. Chung, "Trap-limited and percolation conduction mechanisms in amorphous oxide semiconductor thin film transistors," *Appl. Phys. Lett.*, vol. 98, no. 20, p. 203508, May 2011, doi: 10.1063/1.3589371.

[27] S. Lee, A. Nathan, J. Robertson, K. Ghaffarzadeh, M. Pepper, S. Jeon, C. Kim, I.-H. Song, U.-I. Chung, and K. Kim, "Temperature dependent electron transport in amorphous oxide semiconductor thin film transistors," in *IEEE Int. Electron Devices Meeting (IEDM) Dig. Tech. Papers*, Dec. 2011, pp. 14.6.1–14.6.4, doi: 10.1109/IEDM.2011.6131554.

[28] S. Takagi, A. Toriumi, M. Iwase, and H. Tango, "On the universality of inversion layer mobility in Si MOSFET's: Part I-effects of substrate impurity concentration," *IEEE Trans. Electron Devices*, vol. 41, no. 12, pp. 2357–2362, Dec. 1994, doi: 10.1109/16.337449.

[29] B. G. Streetman and S. Banerjee, *Solid State Electronic Devices*, 6th ed. Englewood Cliffs, NJ, USA: Prentice-Hall, 2005.

[30] H.-J. Kwon, J. Jang, S. Kim, V. Subramanian, and C. P. Grigoropoulos, "Electrical characteristics of multilayer MoS_2 transistors at real operating temperatures with different ambient conditions," *Appl. Phys. Lett.*, vol. 105, no. 15, pp. 152105-1–152105-5, 2014, doi: 10.1063/1.4898584.